

Floating Point Compression of Hierarchical Matrix Formats and its Impact on Matrix-Vector Multiplication

Ronald Kriemann
MPI for Mathematics i.t.S.
Leipzig, Germany
rok@mis.mpg.de

January 30, 2026

Abstract Matrix-vector multiplication forms the basis of many iterative solution algorithms and as such is an important algorithm also for hierarchical matrices which are used to represent dense data in an optimized form by applying low-rank compression. However, due to its low computational intensity, the performance of matrix-vector multiplication is typically limited by the available memory bandwidth on parallel systems. With floating point compression the memory footprint can be optimized, which reduces the stress on the memory sub system and thereby increases performance. We will look into the compression of different formats of hierarchical matrices and how this can be used to speed up the corresponding matrix-vector multiplication.

AMS Subject Classification: 65Y05, 65Y20, 68W10, 68W25, 68P30

Keywords: hierarchical matrices, low-rank arithmetic, data compression, matrix-vector multiplication

1 Introduction

As opposed to sparse matrices, dense matrices have a serious storage problem as the amount of required memory scales quadratically with the number of rows and columns. This translates into an even higher complexity for arithmetic operations. Therefore, certain structural properties of such matrices have been exploited from the very beginning to reduce the memory costs. Low-rank techniques, especially in the form of hierarchical matrices (\mathcal{H} -matrices, [16]), have demonstrated a high efficiency for this in bringing down the storage complexity to (almost) linear levels which furthermore also applies to their arithmetic.

While the linear storage (and compute) complexity is the major factor in reduced storage costs, further optimization is possible for the actual storage format used for representing low-rank data in memory. Here, the double (FP64) or

	Unit Roundoff
FP64	1.11×10^{-16}
FP32	5.96×10^{-8}
TF32	4.88×10^{-4}
BF16	3.91×10^{-3}
FP16	4.88×10^{-4}
FP8 ¹	6.25×10^{-2}

Table 1: Unit roundoff for floating point formats of the IEEE-754 standard and related formats.

single (FP32) precision format is used. However, as low-rank approximation and arithmetic is normally associated with a user defined accuracy, this accuracy is typically much coarser than the unit roundoff of the utilised floating point format shown in Table 1. Therefore, a floating point representation with a precision closer to the low-rank accuracy is wanted to further reduce storage (and possibly computation) costs.

Usually, e.g., [1, 14], this is implemented with *mixed precision* formats, i.e., with hardware supported floating point formats like FP16 or BF16 in addition to FP32 and FP64. A major disadvantage if these formats is the big difference in memory sizes, e.g., two byte for FP16/BF16, four byte for FP32 and eight byte for FP64, which translates into significant precision gaps, e.g., from about 10^{-3} to 10^{-8} to 10^{-16} , which reduces the flexibility in adjusting to the low-rank accuracy.

Hardware provided floating point formats can be used for a special handling of low-rank matrices where parts of the data are stored in different formats [28, 1]. This allows to further reduce memory costs and thereby also increase performance. Nevertheless, also these approaches are limited by the big jumps in memory sizes between such hardware supported floating point formats.

¹Using the E4M3 version of the FP8 format.

Therefore, the scheme in [1] was combined in [22] with general floating point compression methods which allow a much more fine-grained accuracy setting and hence control of memory sizes. Especially for low-rank data this leads to a very efficient storage scheme.

Aside from \mathcal{H} -matrices other hierarchical matrix formats exist like uniform \mathcal{H} -matrices [16, 13] or \mathcal{H}^2 -matrices [17, 10], which use a more advanced low-rank storage scheme with shared or nested bases, requiring only small coefficient matrices for each matrix block. The compression schemes from [22] can also be applied to these matrix formats. The results of this will be investigated in this work.

Standard \mathcal{H} -arithmetic is typically based on dense arithmetic functions defined by the BLAS and LAPACK function set [6]. Therefore, the modified \mathcal{H} -arithmetic in [22] was based on the idea of decompressing all input data of arithmetic kernel functions, executing the arithmetic kernel in standard double precision and then compressing the output data. This way, the actual arithmetic functions remain unchanged. Already this approach showed superior performance for the \mathcal{H} -matrix-vector multiplication (\mathcal{H} -MVM), which is often memory bandwidth limited and as such, any reduction of the memory size will increase performance.

Another reason for this *semi-on-the-fly* approach was the general compression approach in [22], i.e., for floating point data *any* compressor could be used, making it more difficult to optimize access to compressed data.

However, some of the compression schemes in [22] allow random access of entries in the compressed storage and hence, special arithmetic functions can be implemented more easily. The potential benefit of such an approach for \mathcal{H} -matrix vector multiplication for different hierarchical matrix formats will be investigated in this work.

An analogue strategy was used in [7] with the idea of a *memory accessor*, i.e., transparent conversion between a storage and a computation format within a sparse matrix computation. This work is therefore an application of this concept for \mathcal{H} -matrix arithmetic.

For a special floating point compression scheme this is also investigated in [5] for dense and low-rank matrix-vector multiplication with a special focus on performance. We will use an almost identical floating point format also in this work.

The rest of this work is structured as follows: in Section 2 basic definitions and algorithms for \mathcal{H} -matrices in different formats are introduced. Section 3 will discuss different strategies for \mathcal{H} -matrix-vector multiplication. Compression schemes and their application to data within hierarchical matrices and their effect on matrix-vector multiplication will be the topic of Section 4, followed by a conclusion in Section 5.

2 Hierarchical Matrices

2.1 Model Problem

Our model problem is based on a boundary element discretization for the Laplace single layer potential (Laplace SLP).

Let $\Gamma = \{x \in \mathbb{R}^3 : \|x\|_2 = 1\}$ be the domain and $f : \Gamma \rightarrow \mathbb{R}$ a given right-hand side. Then the unknown u is defined by

$$\int_{\Gamma} \frac{1}{\|x-y\|} u(y) dy = f(x), \quad x \in \Gamma \quad (1)$$

Using a triangulation $\Gamma = \cup_{i \in I} \pi_i, I := \{0, \dots, n-1\}$, the function u is replaced by a discrete version $u_h := \sum_{i \in I} u_i \varphi_i$ with (basis) functions

$$\varphi_i(x) := \begin{cases} 1 & x \in \pi_i \\ 0 & \text{otherwise} \end{cases},$$

e.g., piecewise constant ansatz functions over Γ . Using the Galerkin method this results in an equation system with a matrix $M \in \mathbb{R}^{I \times I}$ defined by

$$m_{ij} := \int_{\pi_i} \int_{\pi_j} \frac{1}{\|x-y\|} dx dy \quad (2)$$

The double integral (2) is approximated using quadrature rules described in [29, Chapter 9]. As (2) is non-zero everywhere, M is a dense matrix which will be approximated by low-rank methods.

2.2 \mathcal{H} -Matrices

For the indexset I we define the *cluster tree* as the hierarchical partitioning of I into disjoint sub-sets of I :

Definition 2.1 (Cluster Tree) Let $T_I = (V, E)$ be a tree with $V \subset \mathcal{P}(I)$. T_I is called a cluster tree over I if

1. $I = \text{root}(T_I)$ and
2. for all $v \in V$ with $\text{sons}(v) \neq \emptyset : v = \dot{\cup}_{v' \in \text{sons}(v)} v'$.

A node in T_I is also called a cluster and we write $\tau \in T_I$ if $\tau \in V$. The set of leaves of T_I is denoted by $\mathcal{L}(T_I)$. Furthermore $\text{level}(\tau)$ denotes the (graph) distance of τ from the root I .

Similar to a cluster tree we can extend the hierarchical partitioning to the product $I \times J$ of two index sets I, J , while restricting the possible set of nodes by given cluster trees T_I and T_J over I and J , respectively. Furthermore, the set of leaves will be defined by an *admissibility condition*, which is used to detect blocks in the product tree which can be efficiently approximated by low-rank matrices with a predefined rank k . In the literature, various examples of admissibility can be found, e.g. standard [18], weak [19] or off-diagonal admissibility [15, 2].

Definition 2.2 (Block Tree) Let T_I, T_J be two cluster trees and let $\text{adm} : T_I \times T_J \rightarrow \mathbb{B}$. The block tree $T = T_I \times T_J$ is recursively defined starting with $\text{root}(T) = (I, J)$:

$$\text{sons}(\tau, \sigma) = \begin{cases} \emptyset, & \text{if } \text{adm}(\tau, \sigma) = \text{true} \vee \tau \in \mathcal{L}(T_I) \vee \sigma \in \mathcal{L}(T_J), \\ \{(\tau', \sigma') : \tau' \in \text{sons}(\tau), \sigma' \in \text{sons}(\sigma)\} & \text{else.} \end{cases}$$

A node in T is also called a block. Again, the set of leaves of T is denoted by $\mathcal{L}(T) := \{b \in T : \text{sons}(b) = \emptyset\}$ and $\text{level}(\tau, \sigma) = \text{level}(\tau) = \text{level}(\sigma)$ denotes the distance from the root $I \times J$.

If for a given block tree the rank of the low-rank approximation within admissible blocks can be bounded, one obtains the set of \mathcal{H} -matrices:

Definition 2.3 (\mathcal{H} -Matrix) For a block tree T over cluster trees T_I, T_J and $k \in \mathbb{N}$, the set of \mathcal{H} -matrices $\mathcal{H}(T, k)$ is defined as

$$\mathcal{H}(T, k) := \{M \in \mathbb{R}^{I \times J} : \forall (\tau, \sigma) \in \mathcal{L}(T) : \text{rank}(M_{\tau, \sigma}) \leq k \vee \tau \in \mathcal{L}(T_I) \vee \sigma \in \mathcal{L}(T_J)\}$$

Here, $M_{\tau, \sigma}$ refers to the sub-block $M|_{\tau \times \sigma}$.

In practice the constant rank k is typically replaced by a fixed low-rank approximation accuracy $\varepsilon > 0$ as the resulting \mathcal{H} -matrices are often more memory efficient. For this we assume for an admissible block $M_{\tau, \sigma}$ and its low-rank approximation $U_{\tau, \sigma} V_{\tau, \sigma}^H, U_{\tau, \sigma} \in \mathbb{R}^{\tau \times k'}, V_{\tau, \sigma} \in \mathbb{R}^{\sigma \times k'}$:

$$\|M_{\tau, \sigma} - U_{\tau, \sigma} V_{\tau, \sigma}^H\| \leq \varepsilon \|M_{\tau, \sigma}\|. \quad (3)$$

Here, k' is an ε -dependent rank. This then leads to the definition of the set $\mathcal{H}(T, \varepsilon)$ in an analogue way to $\mathcal{H}(T, k)$ as the set of \mathcal{H} -matrices with local low-rank approximation error ε . We will also use $\mathcal{H}(T)$ if either a fixed rank or a fixed accuracy is used.

Remark 2.4 The set $\mathcal{H}(T)$ also includes various other formats like block low-rank (BLR) [3] with a single hierarchy level or hierarchical off-diagonal low-rank (HODLR) [2] with inadmissibility restricted to the diagonal, as only the clustering or the admissibility condition has to be chosen appropriately.

To simplify the access to certain sub sets of the matrix blocks of a given \mathcal{H} -matrix, some further sets are defined:

Definition 2.5 With $\mathcal{L}(M) := \{M_{\tau, \sigma} : (\tau, \sigma) \in \mathcal{L}(T)\}$ we will denote the set of sub-blocks in M corresponding to leaves in T . For $\tau \in T_I$ the set $\mathcal{M}_\tau^r := \{M_{\tau, \sigma} \in \mathcal{L}(M)\}$ denotes the set of matrix block in the block row defined by τ . In an analogue way the set $\mathcal{M}_\sigma^c := \{M_{\tau, \sigma} \in \mathcal{L}(M)\}$ for the block column is defined. The restriction of both sets to low-rank blocks shall be denoted by $\mathcal{M}_\tau^{r, lr}$ and $\mathcal{M}_\sigma^{c, lr}$, respectively.

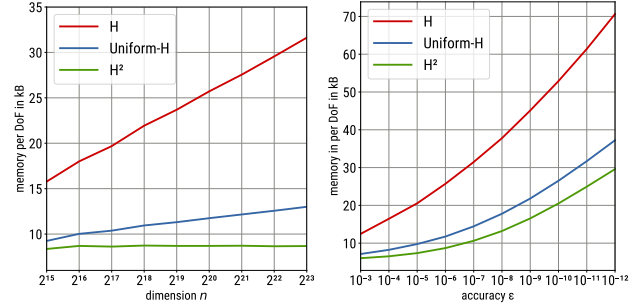


Figure 1: Matrix storage for different \mathcal{H} formats depending on matrix size (left) and accuracy (right).

2.3 Uniform \mathcal{H} -Matrices

In \mathcal{H} -matrices the low-rank blocks are represented in factored form $U_{\tau, \sigma} V_{\tau, \sigma}^H$. Alternatively, one can use $\mathcal{W}_{\tau, \sigma} S_{\tau, \sigma} \mathcal{X}_{\tau, \sigma}$ with orthogonal (row basis) $\mathcal{W}_{\tau, \sigma}$ and (column basis) $\mathcal{X}_{\tau, \sigma}$ and a coupling matrix $S_{\tau, \sigma} \in \mathbb{R}^{k \times k}$, e.g., by computing a QR factorization of $U_{\tau, \sigma} = Q_U R_U$ and $V_{\tau, \sigma} = Q_V R_V$ and setting $\mathcal{W}_{\tau, \sigma} := Q_U, \mathcal{X}_{\tau, \sigma} := Q_V$ and $S_{\tau, \sigma} := R_U R_V^H$. In this case, each low-rank block has individual row and column (cluster) bases. However, for many applications one can find a shared cluster basis \mathcal{W}_τ for all low-rank blocks $M_{\tau, \sigma'} \in \mathcal{M}_\tau^r$ in a single block row. All such cluster bases form a tree $T_{\mathcal{W}} := \{\mathcal{W}_\tau : \tau \in T_I\}$ structurally identical to the cluster tree T_I . For simplicity we assume a cluster basis with rank 0 in case that no low-rank block exists in the corresponding block row. In Figure 2 (center) this can be seen on the two top levels of the cluster bases tree. In an analogue way shared tree column bases $\mathcal{X}_\sigma, \sigma \in T(J)$, and the corresponding tree $T_{\mathcal{X}}$ are defined.

A low-rank block $M_{\tau, \sigma}$ is then represented as

$$M_{\tau, \sigma} = \mathcal{W}_\tau S_{\tau, \sigma} \mathcal{X}_\sigma^H.$$

Such \mathcal{H} -matrices are called uniform \mathcal{H} -matrices (\mathcal{UH} -matrices) and were first introduced together with \mathcal{H} -matrices in [16] and investigated in more detail in [13] where also algorithms for constructing shared cluster bases are presented. While the storage for the coupling matrices, i.e., the actual matrix data, is reduced to $\mathcal{O}(n)$ complexity, the overall memory complexity of \mathcal{UH} -matrices is identical to (standard) \mathcal{H} -matrices due to $\mathcal{O}(n \log n)$ storage for the cluster bases trees $T_{\mathcal{W}}$ and $T_{\mathcal{X}}$. However, in practice memory is often significantly smaller as is shown in Figure 1 where the memory costs for the different matrix formats are presented. Especially noteworthy is the slower increase of the storage for \mathcal{UH} -matrices compared to \mathcal{H} -matrices for an increasing problem size (Figure 1 (left)).

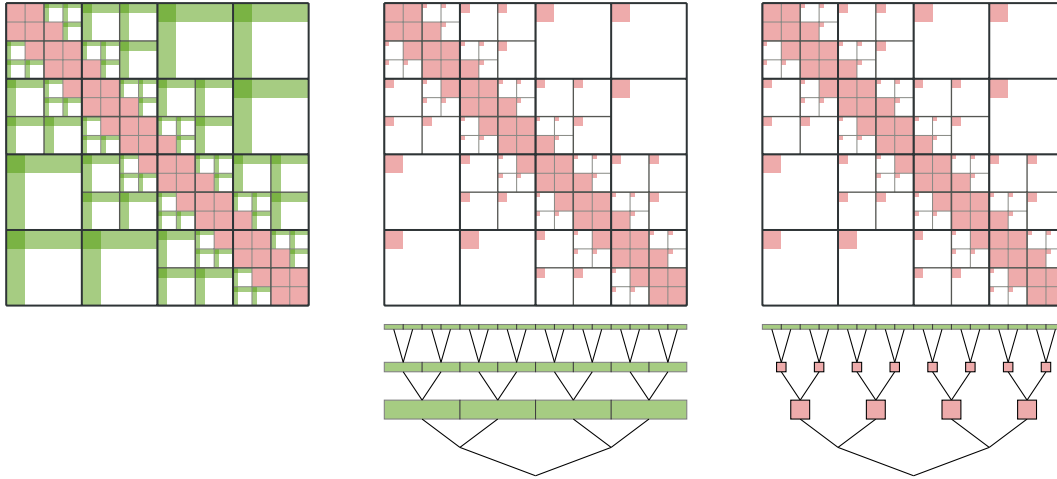


Figure 2: Separate (left), shared (center) and nested (right) cluster bases for \mathcal{H} -matrices, \mathcal{UH} -matrices and \mathcal{H}^2 -matrices.

2.4 \mathcal{H}^2 -Matrices

Further reduction of the storage costs for the cluster bases can be achieved by exploiting the fact that for many applications the bases have a *nestedness* property, i.e., a cluster basis on an upper level can be represented by a linear combination of bases on lower levels of the tree. For this, let $\tau \in T_I$ with two child clusters: $\mathcal{S}(\tau) = \{\tau_0, \tau_1\}$. The cluster basis \mathcal{W}_τ can then be represented as

$$\mathcal{W}_\tau = \begin{pmatrix} \mathcal{W}_{\tau_0} E_{\tau,0} \\ \mathcal{W}_{\tau_1} E_{\tau,1} \end{pmatrix}$$

using the cluster bases $\mathcal{W}_{\tau_0}, \mathcal{W}_{\tau_1}$ from the child clusters and so-called *transfer matrices* $E_{\tau,0}, E_{\tau,1} \in \mathbb{R}^{k \times k}$. Due to the recursive structure of the cluster basis tree, \mathcal{W}_{τ_0} and \mathcal{W}_{τ_1} can again be represented by their corresponding child clusters in the same way until the leaves of the tree are reached. Only there, cluster bases are stored explicitly as for \mathcal{UH} -matrices. For all other bases only the transfer matrices are needed, reducing the per-basis storage from $\mathcal{O}(\tau)$ to $\mathcal{O}(k)$. This is shown in Figure 2 (right).

Representing \mathcal{H} -matrices by such *nested* bases leads to \mathcal{H}^2 -matrices as introduced in [17] and thoroughly discussed in [10]. With this approach the storage complexity for the cluster basis and with this for the full \mathcal{H}^2 -matrix is reduced to linear complexity, which is visible by the constant memory per degree of freedom independent on the matrix size in Figure 1 (left).

3 Matrix-Vector Multiplication

In the following the matrix-vector multiplication for the different formats of hierarchical matrices shall be discussed for the update operation

$$y := \alpha M x + y \quad (4)$$

with an hierarchical matrix M and vectors x and y . The special focus is here on the parallelization of the various algorithms.

Remark 3.1 *All numerical experiments are performed on a single AMD Epyc 9554 CPU with 64 cores and 12 32GB DDR5-4800 memory modules, thereby maximizing the memory throughput of this processor with 12 memory channels. For parallelization Intel TBB v2022.1 was used while Intel oneMKL v2025.1 (sequential version, AVX512 code path) provided the BLAS and LAPACK functions for the uncompressed case. All code was compiled using GCC v14.2. The algorithms described in this work are implemented in the open source software HLR (version c8810d5b)¹.*

3.1 \mathcal{H} -Matrices

The product (4) is computed by iterating over the leaf blocks of M and performing local matrix-vector multiplications, either with a dense matrix for inadmissible blocks or in low-rank format, i.e., $t := V_{\tau,\sigma}^H x|_\sigma$ followed by $y|_\tau := y|_\tau + \alpha U_{\tau,\sigma} t$. The full procedure is shown in Algorithm 1.

Algorithm 1: \mathcal{H} -Matrix-Vector Multiplication

```

procedure hmv( $\alpha, M, x, y$ )
  for  $(\tau, \sigma) \in \mathcal{L}(M)$  do
    if  $(\tau, \sigma)$  is admissible then
       $t := \alpha U_{\tau,\sigma} V_{\tau,\sigma}^H x|_\sigma$ ;
    else
       $t := \alpha D_{\tau,\sigma} x|_\sigma$ ;
     $y|_\tau := y|_\tau + t$ ;

```

Versions of the \mathcal{H} -MVM for parallel systems need to consider load balancing due to different, not a priori known ranks in different low-rank blocks of the \mathcal{H} -matrix if a fixed

¹<http://libhlr.org>, programs: *hmv*, *hmv-uni* and *hmv-h2*

accuracy ε is used. Also the block structure is typically not equal throughout the matrix. This poses a serious scalability issue for the distributed memory case (see [8, 25]) or systems with a NUMA architecture.

On shared memory systems a task-based approach can avoid these problems if the scheduling algorithm is able to assign ready tasks efficiently to idle processors. However, this may lead to other problems as the memory layout of the blocks handled by a single processor may not be optimal for efficient execution. This is of special importance because of the low computational intensity of matrix-vector multiplication, which normally leads to a memory bandwidth limited performance. Different optimization strategies are discussed in [20], where especially the memory layout of the \mathcal{H} -matrix data is adjusted such that memory loads are faster.

Another issue with shared memory programming is handling potential collisions when writing to the same memory positions, e.g., with matrix blocks $M_{\tau,\sigma}$ and $M_{\tau,\sigma'}$ handled by different processors (or processor cores) writing simultaneously to $y|_{\tau}$. In the literature, different solutions to this problem can be found. In [21] *atomic* updates to vector coefficients are used. The implementation in [23] splits the vector y into *chunks* $y|_{\tau}$, $\tau \in \mathcal{L}(T_I)$. Updates to y are then performed for each such chunk separately. Data integrity for parallel updates is ensured by a mutex for each $y|_{\tau}$. This is implemented in Algorithm 2 which replaces the direct update in the last line of Algorithm 1.

Algorithm 2: Chunk based Updates

```

procedure update( $y, \tau, t$ )
  if  $\tau \in \mathcal{L}(T_I)$  then
    lock mutex( $y|_{\tau}$ )
     $y|_{\tau} := y|_{\tau} + t|_{\tau}$ ;
    unlock mutex( $y|_{\tau}$ )
  else
    for all  $\tau' \in \mathcal{S}(\tau)$  do
      update( $y, \tau', t$ )
    
```

Atomic updates and mutexes allow the matrix-vector multiplication to be performed in parallel on the full set of dense and low-rank matrix blocks but depend on the task scheduling scheme for reducing collisions and may suffer from potential performance problems with an increasing number of processor cores. Here, a reduction approach of (thread) local results as is used in [8, 25] may eliminate these problems but again increases the overall memory usage due to multiple copies of the vector data and higher computational costs due to the additional reduction phase, especially for processors with many cores.

An alternative approach is a collision free design in which the memory blocks are scheduled to the processors in a way to prevent simultaneous writing to the same memory positions. For the (non-hierarchical) BLR format with its $p \times q$ set of dense and low-rank sub-blocks this is naturally

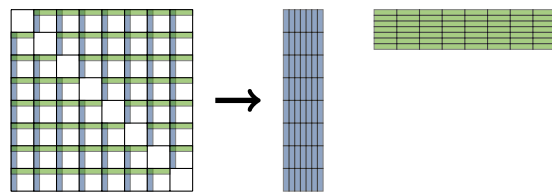


Figure 3: Stacking of low-rank factors for BLR clustering.

achieved by performing the matrix-vector multiplication for all blocks in a single block row in a single task. In [27] this is further optimized by stacking the local low-rank factors of these sub-blocks together as is shown in Figure 3. With this, multiple sub-block matrix-vector multiplications are combined into a single multiplication with an additional exchange of intermediate data. This approach can also be applied to \mathcal{H} -matrices where the low-rank factors of sub-blocks on the *same level* are stacked together (see Figure 4).

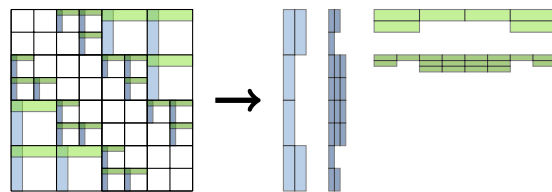


Figure 4: Stacking of low-rank factors per level of the \mathcal{H} -matrix.

A disadvantage of such a stacking method is that the data of low-rank blocks is no longer separate from each other. This makes other \mathcal{H} -matrix computations, e.g., updates during an \mathcal{H} -LU factorization, more difficult especially with non-constant ranks. Furthermore, the intermediate results of the multiplication with the V factors need to be re-assigned to fit the multiplication with the U factors, which induces additional overhead.

Therefore, the original data layout shall be kept while still reordering the sub-block multiplications such that data access collisions are avoided. The basic idea is again to handle matrix-vector multiplication in a single block row sequentially while following the \mathcal{H} -matrix hierarchy from the root to the leaf blocks.

Let $\mathcal{M}^r := \{\mathcal{M}_{\tau}^r : \tau \in T_I\}$ be the set of all block row sets. Since \mathcal{M}^r is defined based on T_I , it can be considered to be structurally identical to the cluster tree. Figure 5 shows this level- and cluster-wise sorting for a simple \mathcal{H} -matrix structure.

Now let $\tau_0, \dots, \tau_{\ell}$ be clusters of T_I with identical level, i.e., $\text{level}(\tau_i) = \text{level}(\tau_j)$, $0 \leq i, j \leq \ell$. Then, for any $0 \leq i, j \leq \ell$ the matrix-vector products in the corresponding sets $\mathcal{M}_{\tau_i}^r$ and $\mathcal{M}_{\tau_j}^r$ can be computed in parallel since $\tau_i \cap \tau_j = \emptyset$.

For any $\tau, \sigma \in T_I$ with $\text{level}(\tau) \neq \text{level}(\sigma)$ the sets \mathcal{M}_{τ}^r and \mathcal{M}_{σ}^r can only be handled in parallel if $\tau \cap \sigma = \emptyset$.

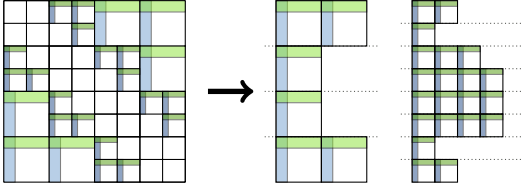


Figure 5: Sorting of \mathcal{H} -matrix blocks per block row and hierarchy level.

However, due to the definition of T_I if $\tau \cap \sigma \neq \emptyset$ then either $\tau \subseteq \sigma$ or $\sigma \subseteq \tau$ holds. Therefore, if T_I is traversed from root to leaves with execution of matrix blocks in a given \mathcal{M}_τ^r before proceeding to the child clusters in $\mathcal{S}(\tau)$, any race condition when accessing y is prevented. This procedure is implemented in Algorithm 3.

Algorithm 3: Parallel \mathcal{H} -Matrix-Vector Multiplication

```

procedure phmvm( $\alpha, \tau, \mathcal{M}^r, x, y$ )
  for all  $M_{\tau, \sigma} \in \mathcal{M}_\tau^r$  do
    if  $\tau, \sigma$  is admissible then
       $y|_\tau := y|_\tau + \alpha U_{\tau, \sigma} V_{\tau, \sigma}^H x|_\sigma$ ;
    else
       $y|_\tau := y|_\tau + \alpha D_{\tau, \sigma} x|_\sigma$ ;
  parallel for  $\tau' \in \mathcal{S}(\tau)$  do
    phmvm( $\alpha, \tau', \mathcal{M}^r, x, y$ )

```

Remark 3.2 Computing the adjoint product $M^H x$ works in an analogue way by iterating over the corresponding block columns.

Remark 3.3 The stacked method for \mathcal{H} -matrices also needs to follow a root-to-leaf approach to prevent collisions when applying the vector update for non-disjoint clusters.

In principle, the computation of all products for matrix blocks in \mathcal{M}_τ^r in Algorithm 3 can be further parallelized using a reduction scheme. One could also combine memory layout optimizations from [20] easily with this approach. However, as no further improvement was observed in practice, such techniques were not used in this work.

In Algorithm 3 no parallelism of the per-matrix-block products, e.g., of $V_{\tau, \sigma}^H \cdot x|_\sigma$ or the product with $U_{\tau, \sigma}$, was considered, which is a major drawback of this procedure if a block structure like HODLR [2] is used. There, the most time consuming computations are performed on the upper levels of the block cluster tree, where only a few processors may be used in parallel. However, as the numerical results below demonstrate, typical \mathcal{H} -matrix block structures do not show these problems, at least not for the number of processors cores considered in this work. Furthermore, such additional parallelization may be easily added to Algorithm 3 if needed.

The runtime performance for the different \mathcal{H} -matrix-vector multiplication algorithms is shown in Figure 6 (left)

for different problem sizes and accuracies. There, “chunks” denotes the mutex based version from [23], “cluster lists” refers to Algorithm 3, the adaptation of the stacked local cluster bases (low-rank factors) for \mathcal{H} -matrices shown as “stacked” and “thread local” uses a matrix-vector multiplication with thread local results which are joined together afterwards.

As can be seen, the runtime of the multiplication using stacked cluster bases is identical to Algorithm 3. Almost identical results are achieved by using mutexes for leaf clusters, indicating that the task scheduling is reasonably efficient on the given system. Only the usage of thread-local vectors increases the runtime, which is mostly due to the additional summation of the thread-local results. Leaving this part out reduces the runtime almost to the same level as for the other methods.

Furthermore, Algorithm 3, bounded by the memory bandwidth, achieves 79% of the peak performance as can also be seen in the roofline plot in Figure 7.

3.2 Uniform \mathcal{H} -Matrices

For \mathcal{UH} -matrices the above algorithm can be applied directly, only the multiplication of low-rank blocks need to be modified from $U_{\tau, \sigma} V_{\tau, \sigma}^H x|_\sigma$ to $\mathcal{W}_\tau S_{\tau, \sigma} \mathcal{X}_\sigma^H x|_\sigma$. However, this would be inefficient as the product $\mathcal{X}_\sigma^H x|_\sigma$ with the column cluster basis is performed multiple times as it needs to be computed for each low-rank block in the same block column. In an analogue way, the product with the row cluster basis \mathcal{W}_τ is performed for each low-rank block in \mathcal{M}_τ^r .

Instead, the multiplication with the cluster basis should be performed only once, yielding coefficient vectors

$$s_\sigma := \mathcal{X}_\sigma^H x|_\sigma$$

of size k which can then be reused for each block in $\mathcal{M}_\sigma^{c, lr}$, i.e., the set of low-rank blocks in \mathcal{M}_σ . This process is named *forward transformation* and shown in Algorithm 4.

Algorithm 4: Forward Transformation for \mathcal{UH} -matrices

```

procedure Forward( $\sigma, x$ )
   $s_\sigma := \mathcal{X}_\sigma^H x|_\sigma$ ;
  for all  $\sigma' \in \mathcal{S}(\sigma)$  do
    Forward( $\sigma', x$ );

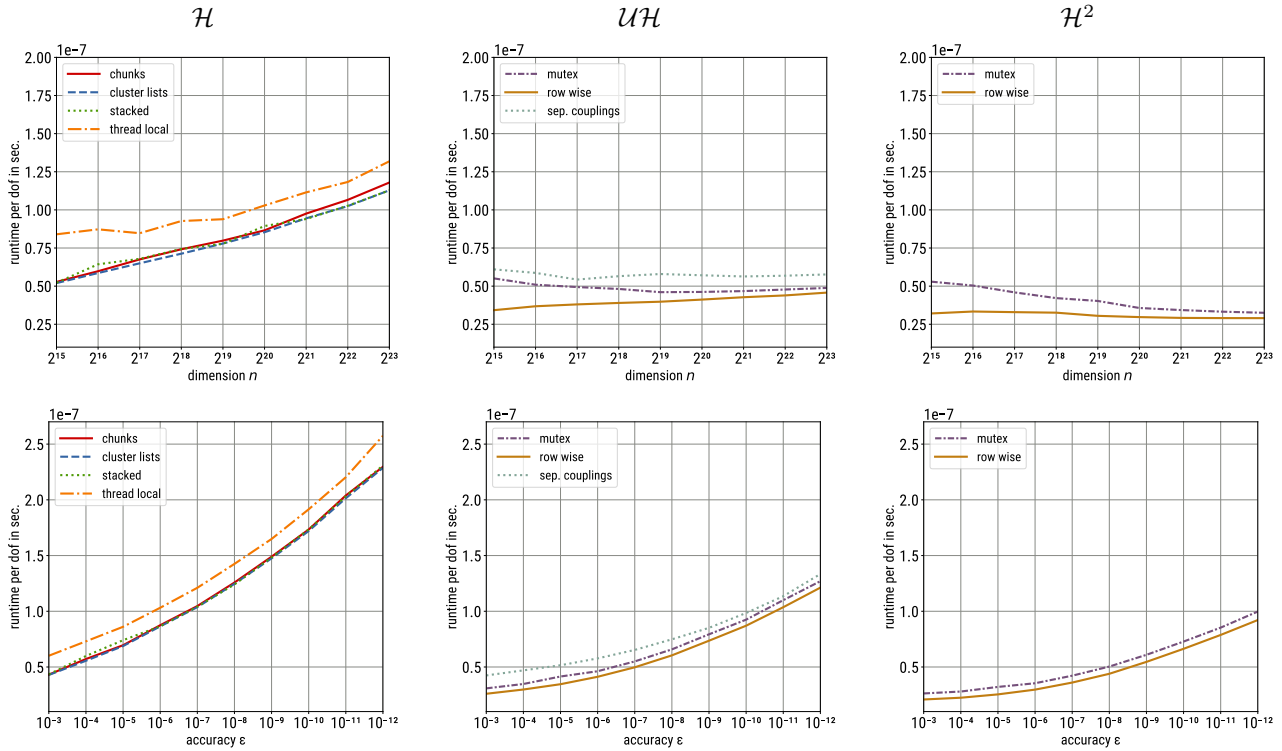
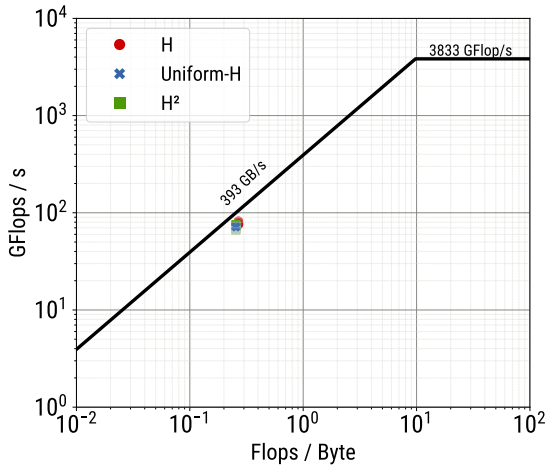
```

Now let

$$t_\tau := \sum_{\sigma, \sigma' \in \mathcal{M}_\tau^{c, lr}} S_{\tau, \sigma} s_\sigma \quad (5)$$

be the accumulated update by all coupling matrices in $\mathcal{M}_\tau^{r, lr}$. The update to y can then be performed in a single step:

$$y_\tau := y_\tau + \mathcal{W}_\tau t_\tau.$$


 Figure 6: Runtime of different matrix-vector multiplication algorithms for \mathcal{H} (left), \mathcal{UH} (center) and \mathcal{H}^2 -matrices (right).

 Figure 7: Roofline plot for \mathcal{H} -MVM, \mathcal{UH} -MVM and \mathcal{H}^2 -MVM.

Thereby also the multiplication with the row cluster bases \mathcal{W}_τ is performed only once, a process also known as *backward transformation*.

For the parallel evaluation of the \mathcal{UH} -matrix-vector product, the same problems as for the \mathcal{H} -matrix case have to be solved, i.e., handling of data races when simultaneously updating identical data blocks. In case of \mathcal{UH} -matrices, the forward transformation is trivially parallelized over all

nodes of the cluster bases tree as all work is on independent data.

This does not hold for the sum in (5). As before for \mathcal{H} -matrices, different strategies for handling this are possible, e.g., guarding updates to t_τ by a mutex, computing (5) in a single task or as a recursive reduction. Again, a mutex would increase the set of parallel tasks to the set of all low-rank blocks in $\mathcal{M}_\tau^{r,lr}$ whereas the latter approach eliminates collisions at the cost of a smaller parallel degree. However, the number of nodes in a typical cluster bases tree should be sufficiently large to ensure no idle times for many-core processors.

Finally, the backward transformation requires further synchronisation between different tasks as overlapping sections of y may be updated simultaneously. As for \mathcal{H} -matrices, this may be solved by mutex guarded updates (in chunks) or by preventing collisions by following the hierarchy from the root to the leaves as in Algorithm 3, i.e., compute the update to y_τ before any updates to $y_{\tau'}$ with $\tau' \in \mathcal{S}(\tau)$. This can also be combined with the computation of (5), which is done in Algorithm 5. There, the set of dense matrix blocks in a given block row is denoted $\mathcal{M}_\tau^{r,d} := \mathcal{M}_\tau^r \setminus \mathcal{M}_\tau^{r,lr}$.

In [13] a different strategy was employed which makes use of a slightly different representation of the coupling matrices $S_{\tau,\sigma}$. Instead of having a single coupling matrix, separate row and column coupling matrices $S_{\tau,\sigma}^r$ and $S_{\tau,\sigma}^c$

Algorithm 5: \mathcal{UH} -matrix-vector multiplication (without forward trans.)

```

procedure UniMVM( $\tau, \mathcal{M}^r, y, x$ )
  for all  $(\tau, \sigma) \in \mathcal{M}_{\tau}^{r,lr}$  do
     $t_{\tau} := t_{\tau} + S_{\tau,\sigma} s_{\sigma}$ ;
   $y' := \mathcal{W}_{\tau} t_{\tau}$ ;
  for all  $(\tau, \sigma) \in \mathcal{M}_{\tau}^{r,d}$  do
     $y' := y' + M_{\tau,\sigma} x|_{\sigma}$ ;
   $y|_{\tau} := y|_{\tau} + y'$ 
  parallel for all  $\sigma' \in \mathcal{S}(\sigma)$  do
    UniMVM( $\sigma', \mathcal{M}^r, y, x$ );

```

with $S_{\tau,\sigma} = S_{\tau,\sigma}^r \cdot (S_{\tau,\sigma}^c)^H$ are used. These matrices are typically obtained during the cluster basis construction for the row and the column cluster bases and are normally combined into a single coupling matrix. Depending on the application the separate storage may lead to a slightly smaller memory footprint for the matrix storage as the rank of the shared cluster basis is typically larger compared to the original rank of a single block.

Furthermore, one can now decouple the product with $S_{\tau,\sigma}$ into two stages. In [13] the first stage consists of computing $(S_{\tau,\sigma}^c)^H s_{\sigma}$ for each low-rank block, which can be done independent from all other blocks and also together with the forward transformation. The second stage consists of performing the product with $S_{\tau,\sigma}^r$ followed by the backward transformation and the update of y . The latter is implemented using thread local data and afterwards combined into the full result.

In all cases the runtime of the \mathcal{UH} -matrix-vector multiplication is in $\mathcal{O}(n \log n)$ (see [13]), especially since the cluster bases storage is in $\mathcal{O}(n \log n)$.

The results of an approach using mutexes for thread synchronization for the per-block products (“mutex”), of Algorithm 5 (“row wise”) and of the version from [13] (“sep. coupling”) are shown in Figure 6 (center). In all presented cases Algorithm 5 yielded the best performance, followed by the mutex based version and the algorithm using separate coupling matrices from [13], the latter again suffering from the additional overhead of combining thread-local results. What is also noteworthy is the performance advantage compared to \mathcal{H} -matrix-vector multiplication. For a fixed accuracy (Figure 6, center, top), also the dependence on the problem size is less than for \mathcal{H} -matrices, demonstrating the more efficient storage scheme of uniform \mathcal{H} -matrices.

On the test system the maximal performance of Algorithm 5 is 78% of the peak performance, as can be seen in Figure 7 and as such is almost identical with the performance for \mathcal{H} -matrices and again limited by the memory subsystem.

3.3 \mathcal{H}^2 -Matrices

The three steps forward transformation, computation of t_{τ} and backward transformation are also present in the \mathcal{H}^2 -matrix-vector multiplication. However, while for \mathcal{UH} -matrices the multiplications with \mathcal{X}_{σ} and \mathcal{W}_{τ} are standard matrix-vector multiplications, the corresponding operations for \mathcal{H}^2 cluster bases are indirect due to its recursive definitions. For the first step we have

$$s_{\sigma} := \mathcal{X}_{\sigma}^H x|_{\sigma} = \sum_{\sigma' \in \mathcal{S}(\sigma)} E_{\sigma'}^H (\mathcal{X}_{\sigma'}^H x|_{\sigma'})$$

which leads to a recursive evaluation of the child cluster bases. Only at the leaves, a direct computation is performed and the resulting coefficients are handed back to the parent cluster bases for updating the corresponding local coefficients via the transfer matrices. This process is performed until the root of the cluster basis tree is reached as shown in Algorithm 6.

Algorithm 6: Forward Transformation for \mathcal{H}^2 -matrices

```

procedure Forward( $\sigma, x$ )
  if  $\sigma \in \mathcal{L}(T_J)$  then
     $s_{\sigma} := \mathcal{X}_{\sigma}^H x|_{\sigma}$ ;
  else
    for all  $\sigma' \in \mathcal{S}(\sigma)$  do
      Forward( $\sigma', x$ );
     $s_{\sigma} := s_{\sigma} + E_{\sigma'}^H s_{\sigma'}$ ;

```

Remark 3.4 *Though Algorithm 6 is very similar to Algorithm 4, the latter can compute all coefficient vectors in parallel while a strict leaves-to-root dependency exists for the \mathcal{H}^2 -matrix version.*

In an analogue way, the backward transformation with the row cluster basis \mathcal{W}_{τ} is evaluated in reverse order, i.e., starting at the root and shifting locally transformed coefficients to child cluster bases until the leaves are reached where the actual update of the destination vector y can be computed. We refer the reader to [10] for a detailed description of the full process.

A cluster basis centric approach to parallelization as is used for \mathcal{UH} -matrices can also be found in the literature for \mathcal{H}^2 -matrices, e.g., in [11] for the distributed memory case or in [12] for GPUs. We adopt Algorithm 5 for \mathcal{H}^2 -matrices, i.e., combine local coupling matrix computations and the backward transformation by following the hierarchy of the row cluster basis. The only change for \mathcal{H}^2 -matrices is the backward transformation which either restricts local coefficients to child clusters or applies the final result to the destination vector. Since updates to y are only performed at the leaf clusters also no race condition exists between simultaneously executed tasks on different processor cores. The result is presented in Algorithm 7.

Algorithm 7: \mathcal{H}^2 -matrix-vector multiplication (without forward trans.)

```

procedure H2MVM( $\tau, \mathcal{M}^r, y, x$ )
  for all  $(\tau, \sigma) \in \mathcal{M}_{\tau}^{r,lr}$  do
     $t_{\tau} := t_{\tau} + S_{\tau, \sigma} s_{\sigma}$ ;
  if  $\tau \in \mathcal{L}(T_I)$  then
     $y' := \mathcal{W}_{\tau} t_{\tau}$ ;
  else
    for all  $\tau' \in \mathcal{S}(\tau)$  do
       $t_{\tau'} := E_{\tau'} t_{\tau}$ ;
    for all  $(\tau, \sigma) \in \mathcal{M}_{\tau}^{r,d}$  do
       $y' := y' + M_{\tau, \sigma} x|_{\sigma}$ ;
     $y|_{\tau} := y|_{\tau} + y'$ 
    parallel for all  $\sigma' \in \mathcal{S}(\sigma)$  do
      H2MVM( $\sigma', \mathcal{M}^r, y, x$ );
    
```

The main advantage of matrix-vector multiplication in the \mathcal{H}^2 -matrix format compared to \mathcal{H} - and \mathcal{UH} -matrices is the runtime of $\mathcal{O}(n)$ (see [10]).

As for \mathcal{UH} -matrices also a mutex based matrix-vector multiplication was implemented, i.e., the updates in (5) to t_{τ} are guarded by a mutex associated to t_{τ} .

Figure 6 (right) shows the results for both versions. The runtime for the \mathcal{H}^2 -matrix-vector multiplication is very similar to the corresponding runtime of the \mathcal{UH} -matrix version. However, the linear runtime and storage complexity of \mathcal{H}^2 -matrices result in a slight advantage compared to \mathcal{UH} -matrices, which should grow for even larger problem sizes. Furthermore, as for \mathcal{UH} -matrices a mutex based approach results in higher runtimes compared to the synchronization free version in Algorithm 7.

As is shown in Figure 7 the maximal performance of Algorithm 7 is about 82% of the peak performance of the test system. This is slightly better compared to the \mathcal{UH} -matrix-vector multiplication and owed to the fact that the forward and backward transformations require significantly less data, thereby reducing the stress on the memory subsystem as this is again a memory bandwidth limited computation.

4 Compressed \mathcal{H} -Matrices

4.1 Floating Point Compression

Floating point data in hierarchical matrices appears in inadmissible blocks as dense matrices holding the coefficients and in low-rank blocks in the form of the low-rank factors or as coupling matrices in \mathcal{UH} - or \mathcal{H}^2 -matrices. Often these are stored in the FP64 (or FP32) format. However, due to low-rank approximation with accuracy ε , already an error is introduced which is typically much larger than the unit roundoff of FP64 (or even FP32).

In [24, 22] the FP64 storage was replaced by error adaptive floating point compression, i.e., an optimized storage format was chosen with a representation error depending

on ε . Different compressors are available to implement such a direct compression of floating point data, e.g., ZFP [26] or BLOSC [9]. Furthermore, different storage schemes based on the IEEE-754 floating point standard were examined.

For one such format (AFLP in [22]) the number of mantissa bits m_{ε} is chosen based on the low-rank approximation error ε as

$$m_{\varepsilon} := \lceil -\log_2 \varepsilon \rceil.$$

Similarly, the number of exponent bits e_{dr} is reduced to meet the *dynamic range* of the data, i.e., the logarithm of the ratio between the largest (v_{max}) and smallest (v_{min}) absolute value:

$$e_{\text{dr}} := \left\lceil \log_2 \log_2 \frac{v_{\text{max}}}{v_{\text{min}}} \right\rceil.$$

The data values are scaled and shifted such that the exponent (including bias) is at least one. This way the lowest e_{dr} bits hold the exponent and can easily be extracted².

While storing just $1 + m_{\varepsilon} + e_{\text{dr}}$ bits per value is space efficient, reading from or writing to memory requires costly bit manipulations. Instead, for AFLP m_{ε} is increased to m'_{ε} such that $1 + m'_{\varepsilon} + e_{\text{dr}}$ is a multiple of 8 which makes memory operations byte aligned.

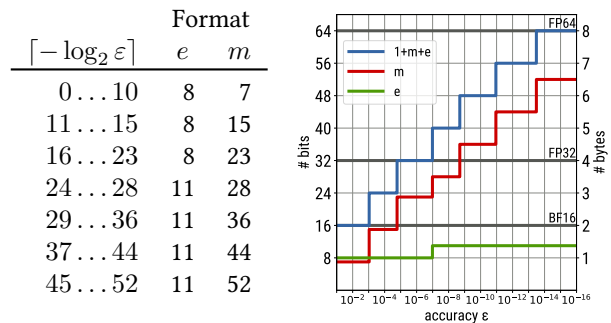


Figure 8: Custom floating point formats based on accuracy

Also discussed in [22] are formats with an adaptive mantissa length but a fixed exponent size of 8 or 11 bits as defined by the FP32/FP64 formats (named SFL and DFL). In [5] this is combined into a single format. Depending on the accuracy the number m of mantissa bits and e exponent bits are chosen such that the resulting format is a byte-aligned, truncated version of the standard FP32 or FP64 formats as is shown in Figure 8. As described in [5] the major advantage of such a scheme is, that conversion to and from FP64 (or FP32) can be done by using fast AVX512 SIMD instructions. In the following we will call this scheme *FPX* (Floating Point eXtended)³. However, in contrast to the rounding strategy employed in [5], where the most significant bit of the truncate is set to 1, round-to-nearest (RTN) is used in this work.

²Also the highest exponent bit is always 1.

³In [5] a common name is missing as each individual (sub) format was considered separately.

Remark 4.1 Since only byte shifting is needed for decompression with FPX, this compression format is up to 50% faster on the test hardware compared to AFLP, which requires floating point addition and multiplication.

Independent on the particular choice of the compression scheme (AFLP or FPX), this so called *direct* compression mode is applied to the dense data of inadmissible blocks. Furthermore, for \mathcal{UH} -matrices and \mathcal{H}^2 -matrices the coupling matrices for each low-rank block are also compressed based on direct compression. This also holds for the transfer matrices of \mathcal{H}^2 -matrix cluster bases. While for the inadmissible blocks this introduces an additional error of ε , this does not affect the overall error of the \mathcal{H} , \mathcal{UH} or \mathcal{H}^2 -matrix as already low-rank approximation was applied with an approximation error of ε per low-rank block. For the same reason does the compression of the coupling matrices in \mathcal{UH} and \mathcal{H}^2 -matrices not increase the overall error. This can be seen in Figure 9, where the error of the compressed matrices vs. an uncompressed (reference) \mathcal{H} -matrix is shown for the AFLP compression. All formats closely follow the predefined approximation error ε .

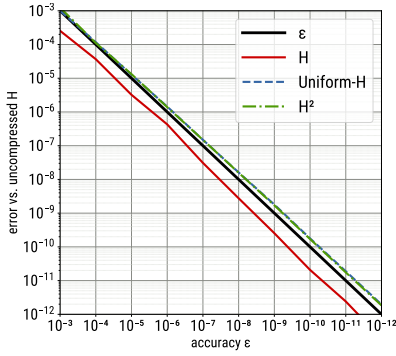


Figure 9: Error of AFLP compressed \mathcal{H} , \mathcal{UH} and \mathcal{H}^2 -matrices compared to reference uncompressed \mathcal{H} -matrix.

4.2 Low-Rank Matrices

As introduced in [4] and combined with general floating point compression schemes in [22], low-rank matrices permit an advanced compression scheme with a Variable Accuracy for each column of the Low-Rank factors (VALR). For a block $M_{\tau,\sigma}$ we assume a rank- k approximation $U_{\tau,\sigma} \cdot V_{\tau,\sigma}^H$ with $\|M_{\tau,\sigma} - U_{\tau,\sigma} V_{\tau,\sigma}^H\|_F \leq \delta$, e.g., $\delta = \varepsilon / \|M_{\tau,\sigma}\|_F$. Using the singular value decomposition we can find orthogonal matrices $W_{\tau,\sigma}$ and $X_{\tau,\sigma}$ and a diagonal matrix $\Sigma_{\tau,\sigma} = \text{diag}(\sigma_0, \dots, \sigma_{k-1})$ with the singular values $\sigma_0 > \sigma_1 > \dots > \sigma_{k-1}$ of $U_{\tau,\sigma} V_{\tau,\sigma}^H$ such that $U_{\tau,\sigma} V_{\tau,\sigma}^H = W_{\tau,\sigma} \Sigma_{\tau,\sigma} X_{\tau,\sigma}^H$.

If the i 'th column w_i of $W_{\tau,\sigma}$ and x_i of $X_{\tau,\sigma}$ are stored with accuracy $\delta_i := \delta / \sigma_i$, resulting in vectors \tilde{w}_i, \tilde{x}_i and

corresponding matrices $\tilde{W}_{\tau,\sigma}$ and $\tilde{X}_{\tau,\sigma}$, then the total approximation error is (see [22, Section 4])

$$\|M_{\tau,\sigma} - \tilde{W}_{\tau,\sigma} \Sigma_{\tau,\sigma} \tilde{X}_{\tau,\sigma}^H\|_F \leq \delta \left(1 + 2k + \delta \sum_{i=1}^k \frac{1}{\sigma_i} \right) \quad (6)$$

With this, any direct floating point compression method can be used to yield an improved storage method for low-rank matrices. The main advantage of this scheme compared to direct compression is, that in the latter case the chosen *fixed* precision is applied to the full data whereas with VALR even for a high accuracy, a low precision may be used for some part of the data.

The cluster bases $\mathcal{W}_\tau \in \mathbb{R}^{\#\tau \times k}$ in \mathcal{UH} or \mathcal{H}^2 -matrices are often computed using the singular value decomposition of some intermediate data, e.g., when combining block-local cluster bases (rf. [10, 13]). With this one typically has as a final step $W_\tau = \mathcal{W}_\tau \Sigma_\tau X_\tau$ for some intermediate matrix W_τ with the singular values again in Σ_τ normally being discarded and only \mathcal{W}_τ being used. However, the singular values allow the application of VALR compression to the cluster bases. For this let $\mathcal{W}_\tau = \{w_0, \dots, w_{k-1}\}$. Furthermore, let $\tilde{\mathcal{W}}_\tau := \{\tilde{w}_0, \dots, \tilde{w}_{k-1}\}$ be a compressed version of \mathcal{W}_τ with $\|w_i - \tilde{w}_i\|_2 \leq \delta_i, 0 \leq i < k$. Then the total error for the compressed cluster basis is

$$\|\mathcal{W}_\tau \Sigma_\tau - \tilde{\mathcal{W}}_\tau \Sigma_\tau\|_F \leq \sum_{i=0}^{k-1} \delta_i \sigma_i = k\delta. \quad (7)$$

When applying the local error per σ_i the additional factor k in (7) is taken into account to compensate for the error increase. In a similar way the factor in (6) is used to adjust local error bounds (rf. [22, Section 4]). The resulting global error stays close to the low-rank approximation error as is visible in Figure 9.

As VALR can be applied to every low-rank block in \mathcal{H} -matrices, it is expected that best compression rates are achieved for this matrix format. In the case of \mathcal{UH} -matrices one can still apply VALR to all cluster bases, whereas for \mathcal{H}^2 -matrices only the leaf cluster bases may be compressed using VALR and therefore are expected to show the least reduction in memory when using compressed storage. This is clearly visible in the results in Figure 10 where the compression ratios for \mathcal{H} -, \mathcal{UH} and \mathcal{H}^2 -matrices are shown for different matrix sizes and accuracies. \mathcal{H} -matrices show the best compression rates, followed by \mathcal{UH} -matrices. What is also notable is that the compression rates increase with the matrix size for \mathcal{H} - and \mathcal{UH} -matrices whereas they stay constant for \mathcal{H}^2 -matrices. For \mathcal{H} -matrices this is due to the increasing portion that low-rank blocks have on the total memory costs, which grows from 67% for the smallest problem size to about 82% for the largest problems.

Finally, in the VALR compression for low-rank blocks, single vectors of the low-rank factors are handled separately and the values within such a vector are typically of

similar magnitude. Therefore, the adaptivity of AFLP for the exponent size is of particular advantage compared to FPX yielding better compression ratios for all matrix formats.

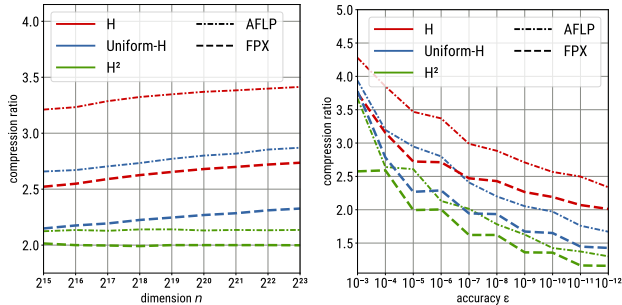


Figure 10: Compression rates of AFLP and FPX depending on matrix size (left) and accuracy (right).

Since compression ratios for the \mathcal{H} and the \mathcal{UH} -format are better compared to the \mathcal{H}^2 -format, the advantage of the latter is reduced with compression enabled. This can be seen in Figure 11, where the ratio of the memory size between the \mathcal{H} - and the \mathcal{UH} -format and the \mathcal{H}^2 -format are shown for uncompressed and compressed storage. For smaller matrix sizes compressed \mathcal{UH} -matrices are even more memory efficient than compressed \mathcal{H}^2 -matrices. Only the better memory complexity of the \mathcal{H}^2 -format leads to less memory for larger matrix sizes. For a varying accuracy, \mathcal{UH} -matrices are almost identical to \mathcal{H}^2 -matrices for the particular matrix size. While storage for \mathcal{H} -matrices does not come as close to the storage of \mathcal{H}^2 -matrices as \mathcal{UH} -matrices do, the advantage of the \mathcal{H}^2 -format compared to the \mathcal{H} -format is significantly reduced.

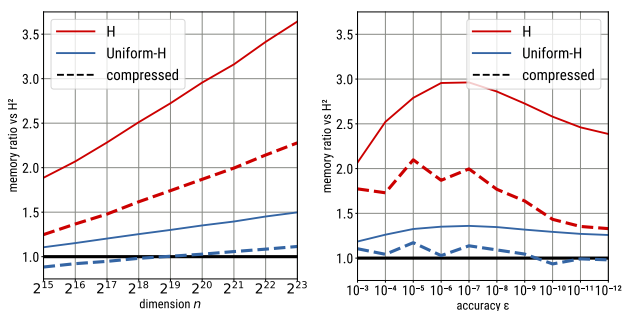


Figure 11: Comparison of memory of uncompressed and compressed \mathcal{H} - and \mathcal{UH} -matrix format with \mathcal{H}^2 -format depending on matrix size (left) and accuracy (right).

Finally, to demonstrate that the technique is not limited to standard \mathcal{H} -matrices, Figure 12 shows the memory sizes and compression ratios for the HODLR and the BLR format when representing the same matrix. Of particular interest is, that the compressed size of both formats is basically

identical, even though HODLR is more efficient in the uncompressed case.

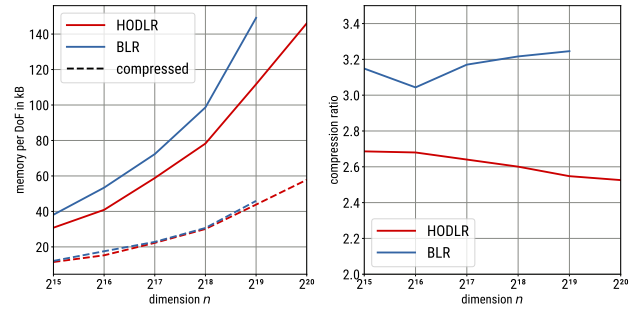


Figure 12: Memory of uncompressed and compressed HODLR and BLR matrices (left) and corresponding compression ratios (right).

4.3 Compressed \mathcal{H} -Matrix-Vector Multiplication

The performance of \mathcal{H} -MVM when using floating point compression was already a (minor) topic of [22]. There, for a dense or low-rank block, the compressed data was first fully converted from the storage format into the compute format and only then the local matrix-vector multiplication was performed. This way, the standard arithmetic (BLAS) kernels, typically optimized by hardware vendors, could be reused. This is more closely investigated in [5] by splitting the compressed data into sub-blocks such that the fast memory close to the processor cores is used in an optimal way.

In [7] the concept of a *memory-accessor* is described which implements on-the-fly conversion between the storage format and the computation format during the arithmetic. The disadvantage of this approach is, that one can not use the optimized BLAS routines but needs to implement special functions in the compressed format. However, as matrix-vector multiplication for \mathcal{H} -, \mathcal{UH} - and \mathcal{H}^2 -matrices is often memory bandwidth limited it may be more forgiving for a (potentially) less heavily optimized implementation. Furthermore, in principle only a single function for dense matrix-vector multiplication is needed in Algorithms 3, 5 and 7 for dense and low-rank blocks, reducing the implementation effort.

In any case, such an approach requires fast access to the compressed values, which holds for the above described compression schemes AFLP and FPX but much less so for ZFP or BLOSC. Furthermore, especially ZFP showed a low decompression performance compared to other formats (see [22]). However, by tightly coupling the compression scheme with the matrix-vector multiplication, any compression format could be used. As such, the restriction to AFLP and FPX in this work should be considered a proof-of-concept.

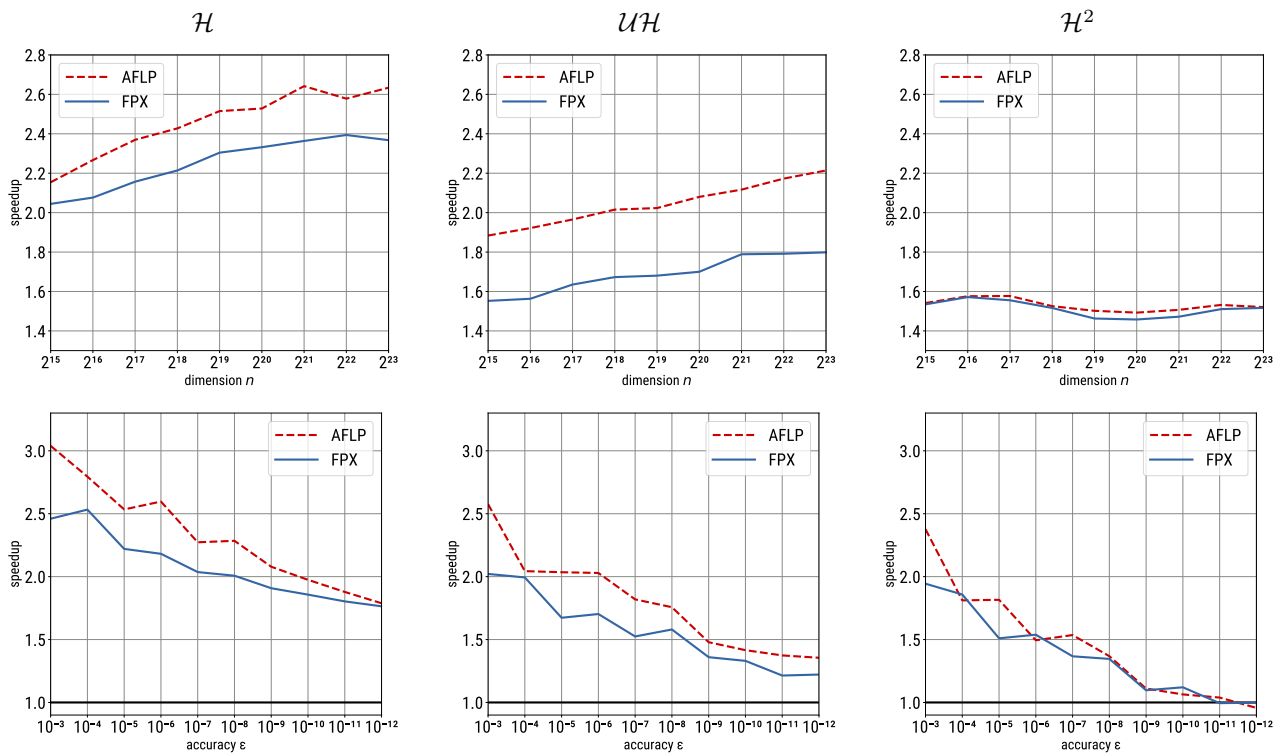


Figure 13: Speedup of compressed matrix-vector multiplication for \mathcal{H} (left), \mathcal{UH} (center) and \mathcal{H}^2 -matrices (right) compared to uncompressed multiplication.

The basic implementation of the compressed dense matrix-vector multiplication required in Algorithms 3, 5 and 7 is shown in Algorithm 8 for the application of a non-transposed $n \times m$ matrix D . It is straight-forward, without particular optimizations, aside from standard code reorganization due to the use of column-major storage scheme. Only the access to the coefficients in D is replaced by the corresponding coefficient decompression.

Algorithm 8: Matrix-vector multiplication with compressed dense $n \times m$ matrix

```

procedure zvmv(in:  $D, x$ , inout:  $y$ )
  for  $0 \leq j < m$  do
    for  $0 \leq i < n$  do
       $y_i := y_i + \text{decompress}(D_{ij})x_j;$ 

```

For the AFLP compression this approach already yielded the best performance. However, when using FPX a block-wise scheme as in [5] showed slightly better results where (up to) 64 contiguous entries of a single column of D are first decompressed into a local buffer.

The results when using Algorithm 8 in \mathcal{H} -, \mathcal{UH} and \mathcal{H}^2 -matrix-vector multiplication are shown in Figure 13. There Algorithms 3, 5 and 7 are used as they showed the best performance in the experiments in Section 3. Results are again presented for an increasing matrix size and a fixed accu-

racy of $\varepsilon = 10^{-6}$ as well as for a fixed problem size and an increasing accuracy. All results are given as speedups compared to the uncompressed \mathcal{H} , \mathcal{UH} and \mathcal{H}^2 -multiplication as shown in Figure 6.

As can be seen, even with this simple implementation the performance improvement with compression is significant with a speedup of about 2x up to 3x for \mathcal{H} -matrices. For \mathcal{UH} -matrices, this reduces to about 1.5x up to 2.5x and is slightly less for \mathcal{H}^2 -matrices. In the latter case, actually no improvement was observed for the highest accuracies. This picture reflects the difference in the reduction of the memory footprint due to compression, which is best for \mathcal{H} -matrices and least for \mathcal{H}^2 -matrices. This also applies to the compression formats: AFLP shows best performance even though the decompression costs are higher compared to the FPX scheme (see Remark 4.1). But since AFLP results in a better memory compression which leads to less bandwidth utilization, the total performance gains are higher.

For all matrix formats the advantage of compressed memory for matrix-vector multiplication reduces with an increasing accuracy but increases with the problem size, with an exception for \mathcal{H}^2 -matrices. This again replicates the compression rate results in Figure 10. However, in all cases the observed speedups are smaller compared to the improvements due to compression, which is at least partly due to the decompression overhead. This overhead is also visible in the

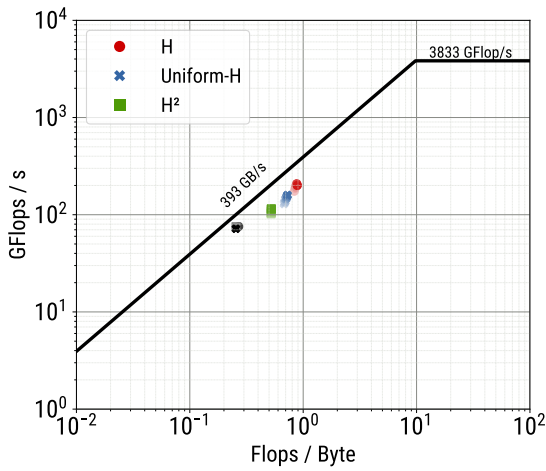


Figure 14: Roofline plot for \mathcal{H} -MVM, \mathcal{UH} -MVM and \mathcal{H}^2 -MVM using AFLP compression.

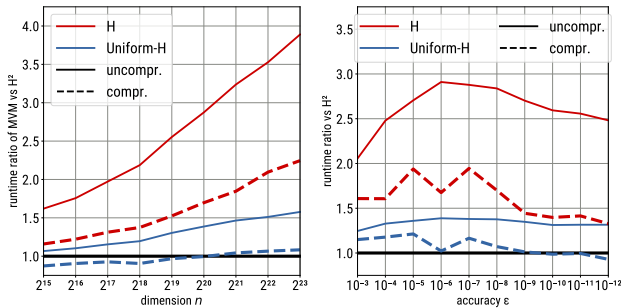


Figure 15: Comparison of runtime of uncompressed and compressed (AFLP) \mathcal{H} - and \mathcal{UH} -matrix matrix-vector multiplication with \mathcal{H}^2 -format depending on matrix size (left) and accuracy (right).

roofline plot in Figure 14. While the overall performance increases, there is a wider gap to the optimal achievable performance than for uncompressed matrix-vector multiplication. Instead of the 80% of the peak performance of the uncompressed multiplication only about 60% are reached with compression enabled.

As for the memory compression, we may further look into the advantage of the \mathcal{H}^2 -matrix format compared to \mathcal{H} - and \mathcal{UH} -matrices for matrix-vector multiplication. Figure 15 shows the ratio of the time for uncompressed and compressed multiplication between \mathcal{H} -matrices/ \mathcal{UH} -matrices and \mathcal{H}^2 -matrices, which represents the performance penalty of the matrix formats compared to the \mathcal{H}^2 -matrix format. This is significantly reduced with compression and brings \mathcal{UH} -matrices very close to \mathcal{H}^2 -matrices for the considered problem sizes and accuracies. However, asymptotically the better runtime complexity of the \mathcal{H}^2 -matrix format will lead to the best performance.

5 Conclusion

Similar to \mathcal{H} -matrices, also the uniform \mathcal{H} -matrix format and the \mathcal{H}^2 -matrix format benefit significantly from an optimized memory representation of the dense and low-rank data. However, this improvement is smaller compared to \mathcal{H} -matrices since the data representation within this advanced formats is already optimized by shared and nested cluster bases. Furthermore, when tightly coupling the compressed format with the matrix-vector multiplication all matrix formats show a noticeable performance speedup compared to the uncompressed case. Though not investigated in this work, these runtime improvements should also apply to similar methods, e.g., triangular vector solves for \mathcal{H} -LU factorizations. Even though a standard model problem was used in the this work, the results should not be limited to this application, though the actual compression rates and thus the performance benefit for matrix-vector multiplication depends on the distribution of singular values within low-rank blocks since these define the permitted accuracy for each low-rank vector pair.

References

- [1] S. Abdulah et al. “Accelerating Geostatistical Modeling and Prediction With Mixed-Precision Computations: A High-Productivity Approach With PaRSEC”. In: *IEEE Transactions on Parallel and Distributed Systems* 33.4 (2022), pp. 964–976. DOI: 10.1109/TPDS.2021.3084071.
- [2] S. Ambikasaran and E. Darve. “An $\mathcal{O}(N \log N)$ Fast Direct Solver for Partial Hierarchically Semi-Separable Matrices”. In: *Journal of Scientific Computing* 57.3 (2013), pp. 477–501.
- [3] P. Amestoy et al. “Improving Multifrontal Methods by Means of Block Low-Rank Representations”. In: *SIAM Journal on Scientific Computing* 37.3 (2015), A1451–A1474. DOI: 10.1137/120903476.
- [4] P. Amestoy et al. “Mixed precision low-rank approximations and their application to block low-rank LU factorization”. In: *IMA Journal of Numerical Analysis* (Aug. 2022).
- [5] P. Amestoy et al. “BLAS-based Block Memory Accessor with Applications to Mixed Precision Sparse Direct Solvers”. working paper or preprint. Apr. 2025. URL: <https://hal.science/hal-05019106>.
- [6] E. Anderson et al. *LAPACK Users’ Guide*. Third. Philadelphia, PA: Society for Industrial and Applied Mathematics, 1999. ISBN: 0-89871-447-8 (paperback).
- [7] Hartwig Anzt, Thomas Grützmacher, and Enrique S. Quintana-Orti. “Toward a modular precision ecosystem for high-performance computing”. In: *International Journal of High Performance Computing Applications* 33.6 (2019), pp. 1069–1078. DOI: 10.1177/1094342019846547.
- [8] M. Bebendorf and R. Kriemann. “Fast parallel solution of boundary integral equations and related problems”. In: *Computing and Visualization in Science* 8.3 (2005), pp. 121–134. DOI: 10.1007/s00791-005-0001-x.
- [9] Blosc Development Team. “A fast, compressed and persistent data store library”. <https://blosc.org>. 2023.

- [10] S. Börm. *Efficient numerical methods for non-local operators. \mathcal{H}^2 -matrix compression, algorithms and analysis*. English. Vol. 14. Zürich: European Mathematical Society (EMS), 2010, pp. ix + 432. ISBN: 978-3-03719-091-3.
- [11] S. Börm and J. Bendoraityte. “Distributed \mathcal{H}^2 -matrices for non-local operators”. In: *Computing and Visualization in Science* 11.4 (2008), pp. 237–249.
- [12] W. Boukaram, G. Turkiyyah, and D. Keyes. “Hierarchical Matrix Operations on GPUs: Matrix-Vector Multiplication and Compression”. In: *ACM Trans. Math. Softw.* 45.1 (Feb. 2019). ISSN: 0098-3500. DOI: 10.1145/3232850.
- [13] K. Bruyninckx, D. Huybrechs, and K. Meerbergen. “Uniform H -Matrix Compression with Applications to Boundary Integral Equations”. In: *SIAM Journal on Scientific Computing* 47.3 (2025), B618–B644. DOI: 10.1137/24M1665209.
- [14] E. Carson, X. Chen, and X. Liu. “Mixed Precision HODLR Matrices”. In: *SIAM Journal on Scientific Computing* 47.3 (2025), A1408–A1435. DOI: 10.1137/24M1683925.
- [15] S. Chandrasekaran et al. “Some Fast Algorithms for Sequentially Semiseparable Representations”. In: *SIAM Journal on Matrix Analysis and Applications* 27 (2 2005), pp. 341–364.
- [16] W. Hackbusch. “A sparse matrix arithmetic based on \mathcal{H} -Matrices. Part I: Introduction to \mathcal{H} -Matrices”. In: *Computing* 62 (1999), pp. 89–108.
- [17] W. Hackbusch, B. Khoromskij, and S.A. Sauter. “On \mathcal{H}^2 -Matrices”. In: *Lectures on Applied Mathematics*. Ed. by H.-J. Bungartz, R.H.W. Hoppe, and C. Zenger. Berlin, Heidelberg: Springer Berlin Heidelberg, 2000, pp. 9–29.
- [18] W. Hackbusch and B.N. Khoromskij. “A sparse \mathcal{H} -matrix arithmetic. Part II. Application to multi-dimensional problems”. In: *Computing* 64.1 (2000), pp. 21–47.
- [19] W. Hackbusch, B.N. Khoromskij, and R. Kriemann. “Hierarchical Matrices Based on a Weak Admissibility Criterion”. In: *Computing* 73.3 (2004), pp. 207–243. DOI: 10.1007/s00607-004-0080-4.
- [20] T. Hoshino, A. Ida, and T. Hanawa. “Optimizations of H -matrix-vector Multiplication for Modern Multi-core Processors”. In: *2022 IEEE International Conference on Cluster Computing (CLUSTER)*. 2022, pp. 462–472. DOI: 10.1109/CLUSTER51413.2022.00056.
- [21] A. Ida, T. Iwashita, T. Mifune, and Y. Takahashi. “Parallel Hierarchical Matrices with Adaptive Cross Approximation on Symmetric Multiprocessing Clusters”. In: *Journal of Information Processing* 22.4 (2014), pp. 642–650. DOI: 10.2197/ipsjip.22.642.
- [22] R. Kriemann. “Hierarchical Low-Rank Arithmetic with Floating Point Compression”. In: *SIAM Journal on Scientific Computing* 47.4 (2025), B763–B784. DOI: 10.1137/24M1649009.
- [23] R. Kriemann. *HLibpro*. URL: <http://www.hlibpro.com/>.
- [24] R. Kriemann et al. “High-Performance Spatial Data Compression for Scientific Applications”. In: *Euro-Par 2022: Parallel Processing*. Ed. by José Cano and Phil Trinder. Cham: Springer International Publishing, 2022, pp. 403–418. ISBN: 978-3-031-12597-3.
- [25] Y. Li, J. Poulson, and L. Ying. “Distributed-Memory \mathcal{H} -Matrix Algebra I: Data Distribution and Matrix-Vector Multiplication”. In: *CSIAM Transactions on Applied Mathematics* 2.3 (2021), pp. 431–459. ISSN: 2708-0579. DOI: 10.4208/csiam-am.2020-0206.
- [26] P. Lindstrom. “Fixed-Rate Compressed Floating-Point Arrays”. In: *IEEE Transactions on Visualization and Computer Graphics* 20.12 (2014), pp. 2674–2683.
- [27] H. Ltaief et al. “Meeting the Real-Time Challenges of Ground-Based Telescopes Using Low-Rank Matrix Computations”. In: *SC21: International Conference for High Performance Computing, Networking, Storage and Analysis*. 2021, pp. 1–14. DOI: 10.1145/3458817.3476225.
- [28] R. Ooi et al. “Effect of Mixed Precision Computing on H -Matrix Vector Multiplication in BEM Analysis”. In: *Proceedings of the International Conference on High Performance Computing in Asia-Pacific Region. HPCAsia '20*. New York, NY, USA: Association for Computing Machinery, 2020, pp. 92–101. ISBN: 9781450372367. DOI: 10.1145/3368474.3368479.
- [29] S. A. Sauter and C. Schwab. *Boundary Element Methods*. Vol. 39. Springer Series in Computational Mathematics. Springer Berlin Heidelberg, 2011. DOI: 10.1007/978-3-540-68093-2-5.